WIMP dark matter through the dilaton portal

Kfir Blum,[a] **Mathieu Cliche,**[b] **Csaba Csáki**[b] **and Seung J. Lee**[c,d]

[a]*Institute for Advanced Study,*
 Princeton, NJ 08540, U.S.A.

[b]*Department of Physics, LEPP, Cornell University,*
 Ithaca, NY 14853, U.S.A.

[c]*Department of Physics, Korea Advanced Institute of Science and Technology,*
 335 Gwahak-ro, Yuseong-gu, Daejeon 305-701, Korea

[d]*School of Physics, Korea Institute for Advanced Study,*
 Seoul 130-722, Korea

 E-mail: kblum@ias.edu, mc863@cornell.edu, csaki@cornell.edu,
 sjjlee@kaist.ac.kr

ABSTRACT: We study a model in which dark matter couples to the Standard Model through a dilaton of a sector with spontaneously broken approximate scale invariance. Scale invariance fixes the dilaton couplings to the Standard Model and dark matter fields, leaving three main free parameters: the symmetry breaking scale f, the dilaton mass m_σ, and the dark matter mass m_χ. We analyze the experimental constraints on the parameter space from collider, direct and indirect detection experiments including the effect of Sommerfeld enhancement, and show that dilaton exchange provides a consistent, calculable framework for cold dark matter with f, m_σ, m_χ of roughly similar magnitude and in the range $\sim 1-10\,\mathrm{TeV}$. Direct and indirect detection experiments, notably future ground-based gamma ray and space-based cosmic ray measurements, can probe the model all the way to dark matter mass in the multi-TeV regime.

Contents

1   Introduction

Embedding the Standard Model (SM) partially or completely in a composite sector can solve the hierarchy problem, by making the Higgs boson composite. Often such a composite sector arises as the low-energy limit of an approximately scale invariant theory, where scale invariance is broken somewhere above the weak scale. If the breaking of scale invariance is spontaneous, then it is accompanied by a light dilaton (the Goldstone boson of spontaneously broken scale invariance) σ that couples to the fields in the composite sector through the trace of the energy-momentum tensor[1] of that sector [2–7]

$$-\frac{\sigma}{f}\mathrm{Tr}T. \tag{1.1}$$

---

[1]To be precise the conserved, symmetric Callan-Coleman-Jackiw energy-momentum tensor [1] of the composite sector.

For massive particles, the coupling to σ is proportional to the particle masses, with the suppression scale f corresponding to the breaking of scale invariance. Similar couplings will be obtained to fields that mix the composite and elementary sector, except in that case the anomalous dimensions of the elementary fields will also appear in the formula. For a detailed discussion of the couplings of dilatons to various fields see [8].

The canonical dilaton Lagrangian (1.1) offers an economical way to couple the SM to new fields that could be singlets under the SM gauge symmetries and thus form an otherwise dark sector. In this paper we study the possibility that dark matter (DM) belongs to such dark sector and couples to the SM through eq. (1.1). In the minimal set up that we explore here, three parameters determine the dynamics of thermal freeze-out in the early Universe: the breaking scale f, the dilaton mass m_σ, and the dark matter mass m_χ. Fixing one of these parameters such that the observed dark matter relic abundance is reproduced leaves a rather predictive framework. We show that a large parametric region exists where the solution is perturbative and produces cold, weakly interacting massive particle dark matter (WIMP), with f, m_σ, m_χ of roughly similar magnitude and in the range $\sim 1 - 10\,\mathrm{TeV}$.

Null results from dark matter direct detection experiments like LUX [9], XENON100 [10] and CDMS [11] put considerable pressure on WIMP models where DM couples to the SM through exchange of SM particles. The annihilation cross section $\sigma_{\mathrm{ann}} \sim 10^{-36}\ \mathrm{cm}^2$, required for WIMP relic abundance consistent with observations, is some ten orders of magnitude larger than the WIMP-nucleon elastic scattering cross section now probed by the direct detection experiments. This excludes Z boson exchange in all but fine-tuned corners of the parameter space, and requires some tuning for Higgs mediation as well. In contrast, the dilaton portal we analyze here quite generically evades the direct detection constraints in the bulk of the relevant parameter space, as the DM coupling to the SM resembles the case of Higgs exchange but with extra suppression of order $(v/f)^2\,(m_h/m_\sigma)^4$ with $v = \langle H \rangle = 246\,\mathrm{GeV}$ and m_σ and the scale f automatically lying in the TeV ballpark to provide the correct relic abundance.

The idea that dark matter could couple to the SM via dilaton exchange was analyzed previously in ref. [12] (where the dilaton was taken to be massless) and in ref. [13] (for some specific warped extra dimensional models where the role of the dilaton was played by the radion). Our work generalizes the results of ref. [13] and extends the analysis of [12] by adding the dilaton mass as a free parameter. This allows a more complete exploration of the parameter space and reveals effects such as Sommerfeld-enhanced annihilation. We also incorporate the most recent experimental bounds from direct and indirect detection as well as collider experiments.

The outline of this paper is as follows. In section 2 we summarize the basic properties of the dilaton. We present its couplings, fixed mainly by the scale f with a few additional parameters characterizing the embedding of the SM matter into the composite sector, comment on expected NDA bounds on the dilaton mass, and present two benchmark models to be studied in the paper. Section 3 contains a calculation of the DM annihilation cross section due to dilaton exchange. After deriving a unitarity bound on the DM mass, we present the parameter space of the theory where the observed relic abundance is reproduced. In section 4 we compare the DM-nucleon scattering cross sections to the experimental bounds

from the latest round of direct detection measurements, finding that large regions of the parameter space are compatible with the bounds. In section 5 we consider constraints from indirect detection of gamma rays and cosmic ray antiprotons. We conclude in section 6. Appendix A summarizes collider bounds on the dilaton, considering LEP, Tevatron and the LHC. Appendix B contains cross-section formulae for the sub-leading annihilation channels that we omit in the body of the text for clarity.

2 The dilaton mediated dark matter model

We start by considering the effective theory describing an approximately scale invariant sector with scale invariance spontaneously broken at the scale f. The Goldstone boson corresponding to this breaking, called the dilaton $\widetilde{\sigma}(x)$, can be parametrized via a spurion field $\Phi(x)$ as [8]

$$\Phi(x) \equiv f e^{\widetilde{\sigma}(x)/f} \tag{2.1}$$

such that under a scale transformation $x \to x e^{\lambda}$ we have $\Phi(x) \to e^{\lambda}\Phi(e^{\lambda}x)$ and $\langle \Phi \rangle = f$. This Φ is not (necessarily) an elementary scalar - rather it is the analog of the Σ field of non-linear σ-models for the case of spontaneously broken scale invariance, which allows one to construct the low-energy effective Lagrangian for the dilaton that captures the essential features of the broken symmetry. To obtain a canonically normalized dilaton kinetic term it is convenient to do a field redefinition such that $\Phi(x) = \sigma(x) + f$ [6] where σ is now the canonically normalized dilaton field. Using a spurion analysis one can then find the low energy theory below the cutoff scale $4\pi f$ by inserting powers of Φ/f in the SM Lagrangian to make it scale invariant. After electroweak symmetry breaking one finds the following effective action describing the interactions of the canonically normalized dilaton with the SM fields [5, 6, 8]

$$\mathcal{L}_{\sigma} = \frac{1}{2}\partial_{\mu}\sigma\partial^{\mu}\sigma - \frac{1}{2}m_{\sigma}^2\sigma^2 - \frac{5}{6}\frac{m_{\sigma}^2}{f}\sigma^3 - \frac{11}{24}\frac{m_{\sigma}^2}{f^2}\sigma^4 + \ldots - \left(\frac{\sigma}{f}\right)\left[\sum_{\psi}(1+\gamma_{\psi})m_{\psi}\bar{\psi}\psi\right] +$$

$$+ \left(\frac{2\sigma}{f} + \frac{\sigma^2}{f^2}\right)\left[m_W^2 W^{+\mu}W_{\mu}^- + \frac{1}{2}m_Z^2 Z^{\mu}Z_{\mu} - \frac{1}{2}m_h^2 h^2\right] + \frac{\alpha_{\text{EM}}}{8\pi f}c_{\text{EM}}\sigma F_{\mu\nu}F^{\mu\nu} +$$

$$+ \frac{\alpha_{\text{s}}}{8\pi f}c_{\text{G}}\sigma G_{a\mu\nu}G^{a\mu\nu}. \tag{2.2}$$

The sum on ψ runs over the SM fermions, which are assumed to be partially composite with light fermions being mainly elementary and the top quark mainly composite. γ_{ψ} corresponds to the anomalous dimension of fermionic operators responsible for generating the SM fermion masses after mixing between the elementary and composite sectors. For composite fermions the anomalous dimension is expected to be small $\gamma_{\psi} \simeq 0$, while for light fermions the anomalous dimension may be sizable.

Naive dimensional analysis (NDA) limits the plausible size of the dilaton mass. For example, considering the dilaton self-energy loop from the trilinear coupling in eq. (2.2) we find that

$$m_{\sigma} \leq 4\pi f \tag{2.3}$$

to ensure that the one-loop correction of the dilaton mass remains below the tree-level mass, and that the couplings of the dilaton to matter remain under control [14]. This is just the reflection of the fact that this theory has an intrinsic cutoff of order $\Lambda \sim 4\pi f$, and we should treat it as an effective theory valid below that scale. Note also that it is difficult to make the dilaton much lighter than the cutoff scale. In generic models there is a tuning of order $\frac{m_\sigma}{\Lambda}$ necessary to lower the dilaton mass [8, 14, 15], though special constructions can potentially alleviate this tuning [16, 17]. We will require that the dilaton is not lighter than $f/10$.[2]

A few additional comments are in order about eq. (2.2). The cubic and quartic dilaton self interaction arise from expanding the effective dilaton potential which includes a scale invariant term, Φ^4, and small explicit sources of scale symmetry breaking such as $\Phi^{4-\epsilon}$. These two terms are expected to be the dominant ones in the effective potential of the non-linear field Φ, and is applicable to all types of theories with spontaneous breaking of scale invariance, irrespective of whether there is an elementary scalar breaking the symmetry, or the breaking happens dynamically. The $\Phi^{4-\epsilon}$ term represents the effect of small explicit breaking of scale invariance. The effect of any explicit breaking term will be to generate a term in the effective potential with power different from 4. If the breaking is small, the power is expected to lie close to 4, hence the usual choice of power $4 - \epsilon$, where ϵ usually represents the anomalous dimension of an explicitly non-scale invariant operator. We want to emphasize again that this parametrization of the potential is expected to be quite general, covering both cases of breaking via an elementary scalar and dynamical breakings of scale invariance. Requiring that $\langle\Phi\rangle = f$ and that $\frac{d^2V(\Phi)}{d\Phi^2} = m_\sigma^2$ fixes the parameters of the dilaton potential. The full expression for the cubic self-coupling of the dilaton is $\frac{5-\epsilon}{6}\frac{m_\sigma^2}{f}$, which for small ϵ we can approximate as $\frac{5}{6}\frac{m_\sigma^2}{f}$,[3] while for small ϵ the quartic is $11/24\frac{m_\sigma^2}{f^2}$. Away from the $\epsilon \to 0$ limit, the prefactor of the cubic coupling can lie anywhere in the interval $[2/6, 5/6]$ [6]. For simplicity, throughout this paper we have used the limiting value $5/6$ for the cubic, though we have verified that this does not influence our results significantly. The coupling of the dilaton to massless gauge bosons arises from two sources; just like for the SM Higgs, the dilaton receives a contribution from top quark and W boson loops, but in addition there is a direct contribution from the trace anomaly. The trace anomaly is proportional to the β-functions: the actual contribution will be the difference between the β-function above and below the symmetry breaking scale. Thus this contribution depends on the details of what fraction of the composite sector is actually charged under the unbroken SM gauge symmetries, and what fraction of the SM fields are composites. For example, the coupling to gluons c_G receives a contribution from the trace

---

[2]Very light dilatons (while generically tuned) can have interesting phenomenology. For example it could be a dark matter component itself, or lead to a form of dark radiation. However in that scenario several additional important cosmological and astrophysical constraints have to be satisfied, including overclosure of the Universe, star and supernova cooling and fifth force constraints. An exploration of these constraints and the viability of the very light dilaton mass region is beyond the scope of this work.

[3]Note that for $\epsilon = 0$ both the mass m_σ^2 and the cubic coupling vanish. Here we are assuming that ϵ is small but non-vanishing.

anomaly and from a top loop and is given by

$$c_G = b_{\text{IR}}^{(3)} - b_{\text{UV}}^{(3)} + \frac{1}{2} F_{1/2}(x_t) \tag{2.4}$$

where $b_{UV,IR}^{(3)}$ are the QCD β-function coefficients above and below the scale f. This is a free parameter of the theory, which gives a measure of the QCD charges of the scale invariant sector. The function $F_{1/2}$ is the usual triangle diagram contribution of a fermion given by

$$F_{1/2}(x) = 2x \left[1 + (1-x) f(x) \right] \tag{2.5}$$

$$f(x) = \begin{cases} \left[\sin^{-1}\left(1/\sqrt{x} \right) \right]^2 & x \geq 1 \\ -\frac{1}{4} \left[\log\left(\frac{1+\sqrt{x-1}}{1-\sqrt{x-1}} \right) - i\pi \right]^2 & x < 1 \end{cases} \tag{2.6}$$

where $x_t = 4m_t^2/m_\sigma^2$ [5, 8]. A similar expression applies to the coupling to photons.

Some of the results in the following sections (in particular the direct detection and collider signals) depend on the parameters c_G and c_{EM}. To this end we define two benchmark model examples which we will study in detail.

Model A: This is the well-studied case proposed in [6] where the entire SM is composite, corresponding to $b_{UV} = 0, b_{IR} = b_{SM}$, giving rise to the parameters $b_{UV}^3 - b_{IR}^3 = -7$, $b_{UV}^{EM} - b_{IR}^{EM} = 11/3$. Note that for a light dilaton these b's depend somewhat on the dilaton mass: for example $b_{UV}^3 - b_{IR}^3 = -11 + 2n/3$, with n denoting the number of quarks whose mass is smaller than $m_\sigma/2$.

Model B: This is a limit of the well-motivated case when only the right-handed top and the Goldstone bosons needed for electroweak symmetry breaking are composite, while we minimize the β-functions of the UV to be as small as possible, resulting in $b_{UV}^3 = b_{UV}^{EM} = 0$, $b_{IR}^3 = -1/3$, $b_{IR}^{EM} = -11/9$. Note however that b_{UV} is in fact a free parameter depending on the actual UV theory, and its value here has been chosen only for illustration.

The final ingredient of the model is χ, the dark matter particle, which can be spin 0, 1/2 or 1. We assume that χ is a composite of the conformal sector, and does not have any direct coupling to the standard model fields which are mainly elementary. The couplings of χ to the dilaton are fixed by a spurion analysis and follow the rules of couplings of generic massive composites [12]:

$$\mathcal{L}_{\text{DM}} \supset \begin{cases} -\left(1 + \frac{2\sigma}{f} + \frac{\sigma^2}{f^2} \right) \frac{1}{2} m_\chi^2 \chi^2 & \text{Scalar} \\ -\left(1 + \frac{\sigma}{f} \right) m_\chi \bar\chi\chi & \text{Fermion} \\ \left(1 + \frac{2\sigma}{f} + \frac{\sigma^2}{f^2} \right) \frac{1}{2} m_\chi^2 \chi_\mu \chi^\mu & \text{Gauge boson.} \end{cases} \tag{2.7}$$

For simplicity we assume that a $\mathcal{Z}_2$ symmetry renders χ to be a stable particle. For the fermionic case, we assume that χ is a Dirac fermion.
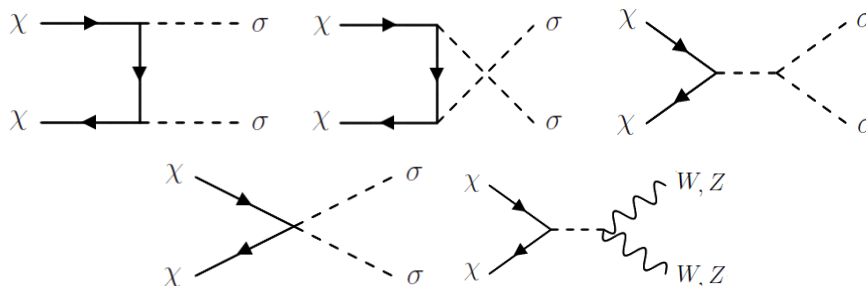
Figure 1. Leading annihilation diagrams of dark matter in the regime $m_\chi \gg m_t$. For fermionic dark matter there is no direct annihilation to dilatons.

3 Relic abundance

In this section we present the calculation of the relic abundance of the dark matter field χ, where annihilations into SM states are assumed to proceed via dilaton exchange, and exhibit the relevant parameter space of the theory. As usual, for small relative velocities v the velocity-weighted annihilation cross section can be expanded as $\sigma v = a + bv^2$. At the freeze-out temperature T_F we have $\langle v^2 \rangle = 6/x_F$ where $x_F = m_\chi/T_F$. The value of x_F can then be determined by solving the Boltzmann equation in an expanding Universe:

$$ x_F = \ln \left(\frac{5}{4} \sqrt{\frac{45}{8}} \frac{g}{2\pi^3} \frac{M_{\mathrm{Pl}} m_\chi (a + 6b/x_F)}{\sqrt{g^*} \sqrt{x_F}} \right), \tag{3.1} $$

where g is the number of degrees of freedom of the dark matter particle and g^* is the effective number of relativistic degrees of freedom in thermal equilibrium during dark matter freeze-out. Once x_F is determined the dark matter relic abundance is given by

$$ \Omega_\chi h^2 \approx \frac{1.07 \times 10^9}{\mathrm{GeV} M_{\mathrm{Pl}} \sqrt{g^*}} \frac{x_F}{a + 3(b - a/4)/x_F}. \tag{3.2} $$

As we show below, the dark matter annihilation cross section (and thus the parameters a, b) in the model considered here is calculated in terms of m_χ, m_σ and f. Requiring that the observed relic abundance $\Omega_\chi h^2 = 0.1199 \pm 0.0027$ [18] is reproduced will thus impose one non-trivial relation and reduce the parameter space of the model. Next we map out this relation in detail, obtaining the reduced parameter space of the theory to be tested by direct and indirect detection experiments as well as collider searches.

3.1 Annihilation cross sections

The dominant dark matter annihilation channels for $m_\chi \gg m_t$ are $\chi\chi \to \sigma\sigma, WW, ZZ$, shown in figure 1. The dominant channels contain factors of m_χ/f, to be compared with all other sub-leading channels (for example s-channel dilaton exchange with quark or higgs final states) that contain factors of m_q/f or m_h/f instead and are thus suppressed by relative powers of $m_{q,h}/m_\chi$. Below we present analytical expressions for the dominant channels in the limit $m_\chi \gg m_t$, for the cases of scalar, fermion and vector dark matter. Formulae for the sub-leading annihilation channels can be found in appendix B. For numerical results all of the allowed annihilation channels are included.

Scalar dark matter. Scalar dark matter annihilation is dominated by s-wave processes. The approximate expressions of the cross sections are

$$\sigma v(\chi\chi \to WW) \simeq \frac{m_\chi m_W^4 \sqrt{m_\chi^2 - m_W^2} \left(2 + \frac{(2m_\chi^2 - m_W^2)^2}{m_W^4}\right)}{2\pi f^4 |4m_\chi^2 - m_\sigma^2 - i\mathrm{Im}\left(\Pi(4m_\chi^2)\right)|^2}, \tag{3.3}$$

$$\sigma v(\chi\chi \to \sigma\sigma) \simeq \frac{m_\chi \sqrt{m_\chi^2 - m_\sigma^2} |2(2m_\chi^2 - m_\sigma^2)^2 + 2m_\sigma^4 - i\mathrm{Im}\left(\Pi(4m_\chi^2)\right)\left(2m_\chi^2 + m_\sigma^2\right)|^2}{16\pi f^4 (2m_\chi^2 - m_\sigma^2)^2 |4m_\chi^2 - m_\sigma^2 - i\mathrm{Im}\left(\Pi(4m_\chi^2)\right)|^2}. \tag{3.4}$$

Note that the second term in the parenthesis of eq. (3.3), corresponding to the formation of longitudinal gauge boson modes, becomes proportional to m_χ^4/m_W^4 in the limit $m_\chi \gg m_W$. In this limit, the m_W^4 pre-factor is cancelled such that the overall cross section scales like m_χ^2/f^4.

In the expressions above $\Pi(p^2)$ is the 1PI self-energy insertion for the dilaton, which on-shell is related to the width via $m_\sigma \Gamma_\sigma = -\mathrm{Im}\left(\Pi(m_\sigma^2)\right)$. Note that we only include the imaginary part in our calculations. The real part (once properly renormalized) is expected to be a moderate correction to the existing real part of the propagator, which will result in small shifts to the precise shape of the contours presented below, but can not qualitatively change the results, as long as the NDA bound (2.3) on the dilaton mass is obeyed. On the other hand properly incorporating the non-vanishing imaginary part can give significant shifts in the resulting cross sections especially close to the resonance.

The total width of the dilaton is the sum of the partial widths to Higgs, quarks, massive gauge bosons and dark matter, which in the limit $m_\sigma \gg m_t$ is dominated by the decays to massive gauge bosons

$$\Gamma_\sigma(\sigma \to WW) = \frac{m_W^4}{4\pi m_\sigma f^2} \sqrt{1 - 4\frac{m_W^2}{m_\sigma^2}} \left(2 + \frac{(m_\sigma^2 - 2m_W^2)^2}{4m_W^4}\right). \tag{3.5}$$

The processes $\chi\chi \to ZZ$ and $\sigma \to ZZ$ are obtained from eqs. (3.3)–(3.5) by replacing m_W by m_Z and dividing by 2 to account for the phase space of identical final state particles. In appendix C we collect the contributions of the other channels to the dilaton decay width.

Fermionic dark matter. For fermionic dark matter, the annihilation channels have no s-wave contribution, thus the dominant contribution is a p-wave process which is suppressed

by a factor of v^2. We find

$$\sigma v(\chi\bar\chi \to WW) \simeq v^2 \frac{m_\chi m_W^4 \sqrt{m_\chi^2 - m_W^2}\left(2 + \frac{(2m_\chi^2 - m_W^2)^2}{m_W^4}\right)}{16\pi f^4 |4m_\chi^2 - m_\sigma^2 - i\mathrm{Im}\left(\Pi(4m_\chi^2)\right)|^2} \tag{3.6}$$

$$\sigma v(\chi\bar\chi \to \sigma\sigma) \simeq v^2 \left[\frac{m_\chi^5 \sqrt{m_\chi^2 - m_\sigma^2}\left(9m_\chi^4 - 8m_\sigma^2 m_\chi^2 + 2m_\sigma^4\right)}{24\pi f^4 \left(16m_\chi^8 - 32m_\chi^6 m_\sigma^2 + 24m_\chi^4 m_\sigma^4 - 8m_\sigma^6 m_\chi^2 + m_\sigma^8\right)} \right.$$
$$+ \frac{25 m_\chi m_\sigma^4 \sqrt{m_\chi^2 - m_\sigma^2}}{128\pi f^4 |4m_\chi^2 - m_\sigma^2 - i\mathrm{Im}\left(\Pi(4m_\chi^2)\right)|^2}$$
$$\left. - \frac{5 m_\chi^3 m_\sigma^2 \sqrt{m_\chi^2 - m_\sigma^2}(5m_\chi^2 - 2m_\sigma^2)}{48\pi f^4 \left(4m_\chi^4 - 4m_\sigma^2 m_\chi^2 + m_\sigma^4\right)} \mathrm{Re}\left(\frac{1}{4m_\chi^2 - m_\sigma^2 - i\mathrm{Im}\left(\Pi(4m_\chi^2)\right)}\right) \right]. \tag{3.7}$$

Vector dark matter. For vector boson dark matter the annihilation is again dominated by s-wave processes:

$$\sigma v(\chi\chi \to WW) \simeq \frac{m_\chi m_W^4 \sqrt{m_\chi^2 - m_W^2}\left(2 + \frac{(2m_\chi^2 - m_W^2)^2}{m_W^4}\right)}{6\pi f^4 |4m_\chi^2 - m_\sigma^2 - i\mathrm{Im}\left(\Pi(4m_\chi^2)\right)|^2} \tag{3.8}$$

$$\sigma v(\chi\chi \to \sigma\sigma) \simeq \frac{m_\chi \sqrt{m_\chi^2 - m_\sigma^2}}{144\pi f^4 (2m_\chi^2 - m_\sigma^2)^2 |4m_\chi^2 - m_\sigma^2 - i\mathrm{Im}\left(\Pi(4m_\chi^2)\right)|^2}\Big(708 m_\chi^8$$
$$+ 44 m_\sigma^2 m_\chi^2 \mathrm{Im}^2\left(\Pi(4m_\chi^2)\right) - 28 m_\sigma^4 \mathrm{Im}^2\left(\Pi(4m_\chi^2)\right) - 1600 m_\sigma^2 m_\chi^6$$
$$+ 1424 m_\chi^4 m_\sigma^4 - 576 m_\sigma^6 m_\chi^2 + 11 m_\sigma^4 \mathrm{Im}^2\left(\Pi(4m_\chi^2)\right) + 96 m_\sigma^8\Big). \tag{3.9}$$

3.2 Unitarity considerations

We emphasize again that the WW and ZZ annihilation channels are important because of the enhanced contributions of the longitudinal modes. Note that ref. [12] neglected these channels due to the suppression of the W/Z couplings by $m_{W,Z}/f$. However as we have shown in the previous section, these factors are cancelled in the limit $m_\chi \gg m_Z$ due to the contributions of the longitudinal modes which grow with the CM energy/dark matter mass.

For large DM mass, the gauge boson longitudinal modes might violate unitarity. This is analogous to the unitarity violation in elastic WW scattering in the standard model without the Higgs. However here the Higgs does not save unitarity. Thus we will have a unitarity bound on the DM mass, related to the built-in cutoff for the theory above which it is expected to be strongly coupled. One can estimate the unitarity bound on m_χ by considering the contribution of the longitudinal mode to the scattering amplitude in the large DM mass limit, given by $\mathcal{M} \approx 2m_\chi^2/f^2$ for either scalar, fermion or vector DM. The resulting s-wave partial wave amplitude $a_0 \approx m_\chi^2/(16\pi f^2)$ satisfies the unitarity bound $|\Re(a_0)| \leq 1/2$ if

$$m_\chi \leq \sqrt{8\pi} f. \tag{3.10}$$

This unitarity bound on m_χ is slightly more constraining than the NDA estimate for the cutoff $m_\chi \lesssim \Lambda_{NDA} = 4\pi f$. A similar analysis for the annihilation to dilatons results in the same upper bound.

3.3 The basic parameter space

We now analyze the parameter space of the model that is compatible with the observed dark matter relic density. Figure 2 shows the available parameter space where the observed relic density can be reproduced by an appropriate choice of the symmetry breaking scale f. The top left, top right, and bottom panels show the results for scalar, fermion, and vector dark matter, respectively. The x- and y-axes correspond to the dilaton and dark matter mass, while the contours show the value of f that is required to obtain the observed dark matter relic density.

For concreteness, in the rest of this section we discuss the scalar dark matter case. We later summarize the results for fermion and vector dark matter. To understand the results shown in figure 2 (top left, as we are focusing on the scalar example), we consider the different parametric regions in turn. Consider the case $m_\chi, m_\sigma \gg m_Z$, where annihilation to WW, ZZ and, if kinematically allowed, $\sigma\sigma$ dominates. Assume first $m_\chi > m_\sigma$, corresponding to the upper-left region in figure 2. Here we have

$$\langle \sigma v \rangle \approx \frac{m_\chi^2}{4\pi f^4} \approx 3 \times 10^{-26} \left(\frac{f}{6\,\text{TeV}} \right)^{-2} \left(\frac{m_\chi}{f} \right)^2 \text{cm}^3/\text{s} \qquad (\text{valid for } m_\chi \gg m_\sigma). \ (3.11)$$

Recall that relic abundance consistent with observations requires $\langle \sigma v \rangle \approx 3 \times 10^{-26}$ cm^3/s, and that $\Omega_\chi h^2 \propto \langle \sigma v \rangle^{-1}$, imposing the relation $m_\chi = f^2/(6\text{TeV})$. Combining this with the unitarity bound $m_\chi \sim \sqrt{8\pi} f$ obtained above, we find an upper bound $f < 30\,\text{TeV}$. Violating this bound leads to DM annihilation cross section that is too small, and so DM relic density that is too high to match observations. A caveat in this derivation is that our dark matter particle may co-annihilate with extra particles in the dark sector. If this co-annihilation is efficient, due to some mass degeneracy in the dark sector and large cross sections, then it would relax the bound on f, allowing f to be somewhat larger than 30 TeV. Even taking this caveat into account, a rough bound $f \lesssim 100\,\text{TeV}$ is still expected to hold. We note that this derivation of the bound on f is compatible with the unitarity argument of [19], that showed that $m_\chi \lesssim 100\,\text{TeV}$ is required in general from S-matrix unitarity (we update their early result here by using the currently measured DM relic density). Plugging the model-independent upper bound on m_χ from ref. [19] into eq. (3.11), we obtain again $f \lesssim 30\,\text{TeV}$. The consistency between eq. (3.10) and the unitarity bound of [19] implies that eq. (3.10) is satisfied throughout the parameter space shown in figure 2.

Next, consider the region with $m_\sigma \gg m_\chi$, so that the $\chi\chi \to \sigma\sigma$ channel is kinematically forbidden. This region corresponds to the lower-right part of figure 2. In this regime, and still assuming $m_\chi \gg m_Z$, one finds the following approximate form for the cross section:

$$\langle \sigma v \rangle \sim \frac{3m_\chi^6}{\pi f^4 m_\sigma^4} \approx 2 \cdot 10^{-26} \left(\frac{m_\chi}{350\,\text{GeV}} \right)^6 \left(\frac{\text{TeV}}{f} \right)^4 \left(\frac{\text{TeV}}{m_\sigma} \right)^4 \text{cm}^3/\text{s} \quad (m_\chi \gg m_W, \, m_\sigma \gg m_\chi).$$
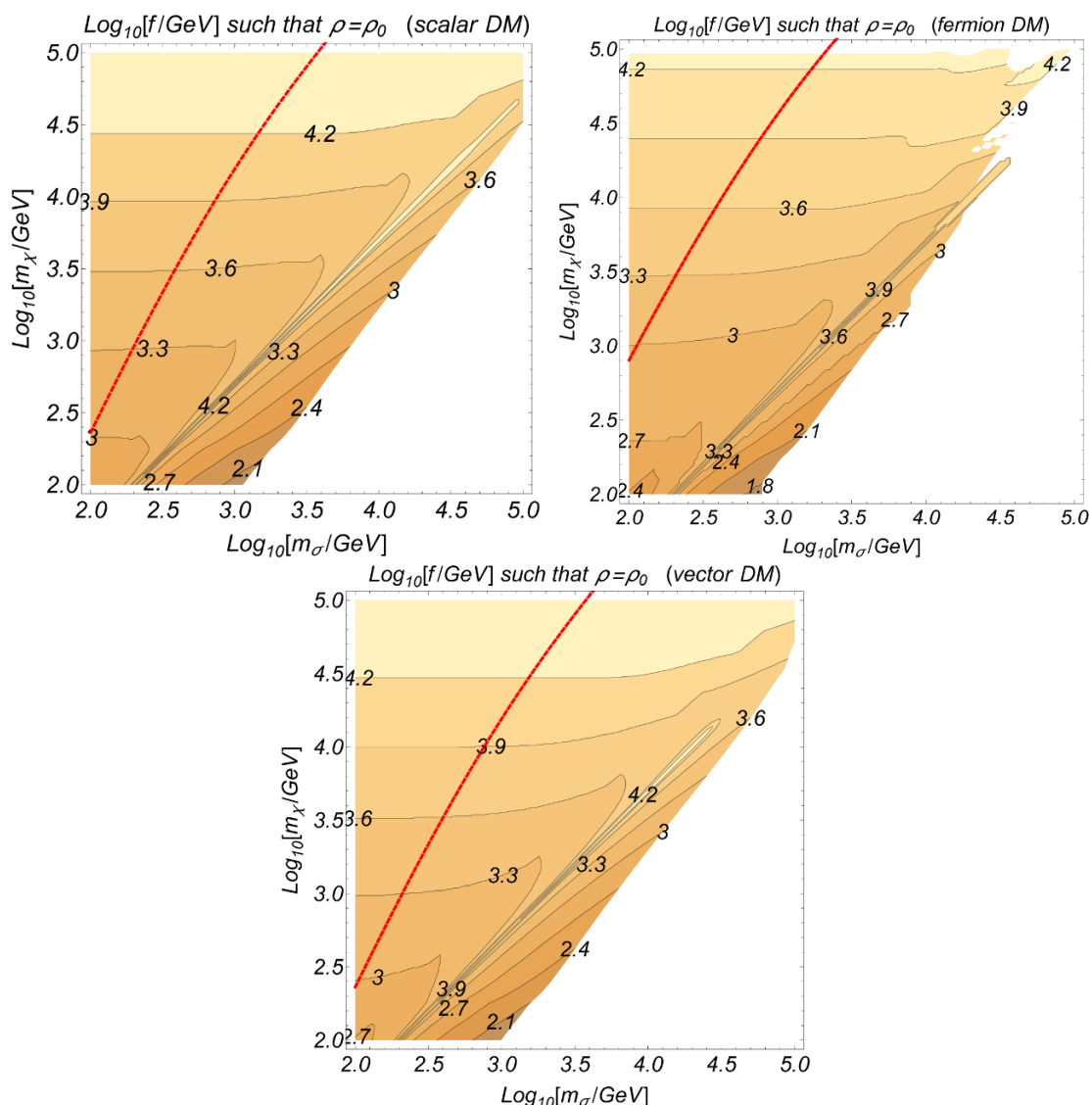$$(3.12)$$

Figure 2. Parameter space for scalar (top left), fermion (top right) and vector (bottom) dark matter with freeze-out mediated by dilaton exchange. The x and y axes correspond to the dilaton and dark matter mass, respectively. Contours show the value of the symmetry breaking scale f, that is required in order to obtain the observed dark matter relic density. In the blank region in the lower-right part of the plot, there is no real solution for f that provides the correct relic density while satisfying eq. (2.3). Above the red dashed line $m_\sigma < f/10$, signaling some degree of fine-tuning. Note that the model-independent unitarity bound of ref. [19] implies $m_\chi \lesssim 10^5$ GeV (see text).

As one increases the dilaton mass m_σ the symmetry breaking scale f needs to decrease in order to keep the relic abundance fixed. However, one will very quickly need to lower f below the value $m_\sigma/4\pi$, implying that we have left the regime of validity of our effective theory. Therefore most of the lower left region will be excluded based on this criterion. Of course the exact shape of the excluded region will be somewhat uncertain: it depends on the exact onset of strong coupling, and can also be slightly modified by strong co-annihilations in the dark sector. Nevertheless, even in this case we expect that the allowed region would shift only slightly.

The resonance at $m_\sigma = 2m_\chi$ is clearly visible in figure 2. The approximate expression of the cross section close to the resonance region is

$$\langle \sigma v \rangle \sim \frac{3m_\chi^6}{\pi \left[(\Delta m)^4 f^4 + \frac{9m_\chi^8}{4\pi^2} \right]} \, , \qquad (3.13)$$

where $\Delta m^2 = 4m_\chi^2 - m_\sigma^2$, measuring the deviation from the exact location of the resonance. In this region (but above the blank region corresponding to eq. (3.12)), a large value of f is required to reduce the otherwise too high annihilation cross section. Note, that once $m_\chi \sim 40\,\text{TeV}$ the cross section falls below the observed value even without a contribution from the resonance. Above those masses one does not expect any more resonant behavior, which is indeed what is reflected in figure 2. We note that numerical resolution affects the size of f that is displayed in figure 2 exactly on the resonance line, as $f \to \infty$ for $\Delta m^2 \to 0$. Of course, living exactly on resonance corresponds to an extremely fine-tuned parametric set-up. Note that beyond the mere parametric fine-tuning, another issue here is that $f \gg m_\sigma$ would imply dynamical fine-tuning as well.

We conclude the discussion of the scalar DM case by considering the scenario proposed in ref. [8], that entertained the possibility of having the newly discovered Higgs-like particle itself be the dilaton. For the dilaton to mimic the Higgs, we must have $m_\sigma \approx m_h = 126\,\text{GeV}$ and $f \approx v = 246.2\,\text{GeV}$. For these values of m_σ and f, we find that the dark matter mass that is needed for correct relic abundance is $m_\chi \approx 52\,\text{GeV}$ if the dark matter is a scalar. The leading annihilation channels at this value of m_χ are to bottom and charm quarks and tau leptons. Larger values of m_χ result in relic abundance that is too low, while lower values of m_χ give a too-high relic abundance. This means that $m_\chi \approx 52\,\text{GeV}$ is an upper bound for scalar dark matter mass in our framework in the Higgs-like dilaton scenario. As we show in section 4, such a low scalar dark matter mass is excluded by direct detection limits. Similar results are obtained for the case of fermion and vector DM, as presented in the second and third plots in figure 2. The higgs-like dilaton scenario would require fermion dark matter of 61 GeV, or vector DM of 56 GeV. As we will see both of these cases are excluded by the direct detection bounds.

Finally, note that in part of the parameter space depicted in figure 2 the DM annihilation cross section receives large non-perturbative corrections at low center of mass velocities (Sommerfeld enhancement). In our model, at large DM mass when the effective coupling m_χ/f is not far from the perturbativity limit, the effect induces a sizable correction to the relic abundance calculation. We compute the Sommerfeld enhancement in section 5

and include it in a simplified form in the calculation of figure 2, by rescaling the tree-level annihilation cross section by the Sommerfeld enhancement factor at relative DM velocity $v = 0.3$, corresponding roughly to the thermal freeze-out kinematics. In most of the parameter space, corresponding to perturbative coupling $(m_\chi/f)^2/4\pi \ll 1$, the correction to the derived value of $f(m_\chi, m_\sigma)$ fixed by the relic abundance requirement is insignificant.[4]

4 Direct detection

Having defined the parameter space of the theory that reproduces the correct relic abundance, we now study direct detection constraints. For direct detection we need to consider the elastic cross section of a dark matter particle that scatters off a nucleon. The dilaton interacts with quarks q and the gluons $G^{a\mu\nu}$ inside a nucleon [21, 22]. Thus the relevant part of the dilaton effective Lagrangian is

$$\mathcal{L} \supset -\sum_q \frac{\sigma}{f}(1 + \gamma_q)m_q q\bar{q} + \frac{\alpha_s}{8\pi f}c_G G^2 \,. \tag{4.1}$$

To estimate the anomalous dimension for quarks, one can consider the corresponding warped extra dimensional models where the anomalous dimension is determined [5] by $1 + \gamma = c_L - c_R$, where $c_{L,R}$ are the bulk fermion mass parameters. For typical warped fermion scenarios we find for example $\gamma_s \sim 0.16$, which we neglect in the bounds below.

Taking the matrix element between nucleon states yields the effective nucleon-dilaton Lagrangian

$$\mathcal{L}_{\sigma nn} = y_n \sigma n\bar{n} \tag{4.2}$$

where the coefficient y_n is determined by the f_q^n, R^n hadronic matrix elements:

$$y_n \equiv -\sum_q f_q^n \frac{m_n}{f} + R^n \frac{c_G}{8\pi f} \,. \tag{4.3}$$

For these matrix elements we use the values from [22–24]:

$$
\begin{aligned}
f_q^n &= \langle n|\bar{q}q|n\rangle \frac{m_q}{m_n} \\
f_u^n &\simeq f_d^n \simeq 0.022 \\
f_s^n &\simeq 0.043 \\
f_c^n &\simeq 0.0814 \\
f_b^n &\simeq 0.0785 \\
f_t^n &\simeq 0.0820 \\
R^n &= \alpha_s \langle n|G_{\mu\nu}^a G^{a\mu\nu}|n\rangle \simeq -2.4\text{GeV}
\end{aligned} \tag{4.4}
$$

---

[4]In fine-tuned regions of the parameter space, where the Sommerfeld effect hits a resonance, DM annihilation re-coupling can significantly affect the relic abundance calculation [20]. We ignore this effect here and comment about it in section 5.

With this effective interaction the scattering cross section between dark matter and nucleons is given by

$$\sigma_{\chi,n} \approx \frac{y_n^2}{\pi} \left(\frac{m_\chi}{f} \right)^2 \frac{m_n^2}{m_\sigma^4} \tag{4.5}$$

for either scalar, fermionic or vector dark matter.

Fixing the scale f for given m_σ and m_χ to match the relic abundance, we plot the DM-nucleon elastic scattering cross section as a function of the dark matter mass for a few dilaton mass values. The results are illustrated on figure 3 along with the recent direct detection constraints from the LUX experiment [9]. We have also included the effects of the collider bounds on the dilaton from the LHC and other machines (see appendix A). These plots show that most of the parameter space is currently allowed both by the dark matter direct detection experiments and also by the collider constraints, as long as $m_\sigma \gtrsim 200\,\text{GeV}$.

As discussed in section 3.3, for $m_\chi \gg m_t$ and away from the resonance the annihilation cross section is proportional to m_χ^2/f^4. Moreover, since $y_n \propto 1/f$, we can see that the elastic scattering cross section is proportional to the same combination m_χ^2/f^4. Thus in the appropriate regime the elastic cross section will be independent of the dark matter mass, as can be seen in figure 3.

5 Sommerfeld enhancement and indirect detection

We now consider the prospects for indirect detection of dark matter annihilation via gamma ray and cosmic ray antiproton flux measurements.[5] We limit the discussion to the case in which the DM χ is a real scalar field. We expect similar results for the vector DM case; the fermion DM case will not have significant cosmic ray signatures as its annihilation is p-wave suppressed in the small virial velocity of the Milky Way and its dwarf satellite galaxies.

The parameter space of interest for the model includes the regime where $m_\chi > m_\sigma$. In this regime, dilaton exchange produces an attractive Yukawa potential $-\frac{\alpha}{r}e^{-m_\sigma r}$, with $\alpha = \frac{m_\chi^2}{4\pi f^2}$, that affects the dark matter annihilation process giving rise to Sommerfeld enhancement (SE; see e.g. [26, 27]) that needs to be taken into account in the indirect detection estimates. In the top panel of figure 4 we plot the effective SE factor (denoted SE_{eff}) in the $\{m_\sigma, m_\chi\}$ plane, fixing the value of the scale f at each point to match the observed dark matter relic abundance. We define SE_{eff} as the value of the SE today in the Galactic halo, normalized to its value during DM freeze-out when $v \sim 0.3$. In our

---

[5]Additional constraints can be derived from neutrino experiments. These constraints are typically weaker than those arising from gamma ray and antiproton data (see e.g. [13] for discussion of the ν flux in the context of a related model) and we do not consider them in this work. Under specific cosmic ray propagation model assumptions, constraints can also be derived from the high energy positron flux. In comparison to the $\bar{p}$ calculation, however, the theoretical uncertainties for e^+ are larger as the results depend crucially on the cosmic ray propagation time in the Galaxy that dictates the amount of e^+ radiative energy loss [25], and so we do not consider e^+ constraints in this work.
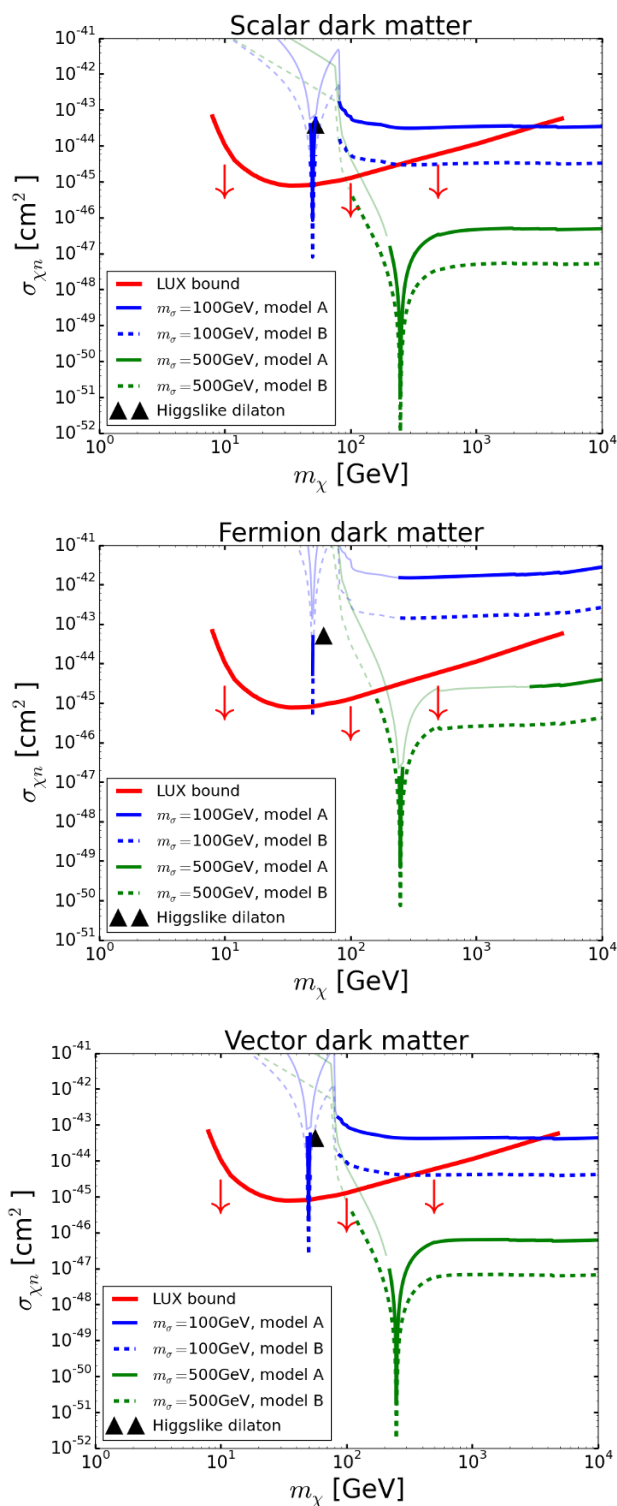
Figure 3. Nucleon-dark matter elastic cross section as a function of dark matter mass. The red arrows point towards the non-excluded region. The lighter portion of the curves are already excluded by bounds from collider experiments searching for a dilaton.

calculation we use an approximate formula for the SE factor [20, 28, 29],

$$SE \approx \frac{\pi}{\epsilon_v} \frac{\sinh\left(\frac{12\epsilon_v}{\pi\epsilon_\phi}\right)}{\cosh\left(\frac{12\epsilon_v}{\pi\epsilon_\phi}\right) - \cos\left[2\pi\sqrt{\frac{6}{\pi^2\epsilon_\phi} - \left(\frac{12\epsilon_v}{\pi\epsilon_\phi}\right)^2}\right]}, \qquad (5.1)$$

where $\epsilon_v \equiv \frac{v}{2\alpha} = \frac{2\pi v f^2}{m_\chi^2}$ and $\epsilon_\phi \equiv \frac{m_\sigma}{\alpha m_\chi} = \frac{4\pi m_\sigma f^2}{m_\chi^3}$. We set the value of the dark matter particles' relative velocity to $v = 10^{-3}$, appropriate for annihilation in the Galactic halo. We have verified that the approximation above reproduces the full Sommerfeld calculation to a good accuracy.

The top panel of figure 4 shows that for DM mass above a few TeV, large values of the SE factor are possible with $SE_{\text{eff}} > 10^2$ in resonance regions. As we show below, this result may have interesting implications — striking indirect detection signatures are possible if the model happens to live at an SE resonance. However, resonant SE is limited to fine-tuned regions in the parameter space. To illustrate this point, in the bottom panel we plot the value of SE vs. the DM mass fixing $m_\sigma = 3\,\text{TeV}$ (corresponding to a vertical slice through the center of the top panel, marked by an arrow). For generic parameter configuration the effective SE factor is modest, and only grows above 10^2 near resonances and for extremely heavy DM mass, close to the unitarity limit where our calculation breaks down. Note that we truncate the value of SE_{eff} at 10^3 in resonance peaks. As the resonance regions are fine-tuned, this has limited impact on our analysis. According to the analysis of [20], the relic abundance is depleted at the tip of these SE resonances due to chemical re-coupling of DM at low redshifts, an effect that we do not include here and that would reduce the value of SE_{eff}. In addition, the low velocity divergence of the SE at the resonance tip should be regulated by bound-state decay that would also suppress the peak SE.

In sections 5.1 and 5.2 below we calculate antiproton and gamma ray constraints on the model. For antiprotons we adopt a conservative model-independent approach to the problem of cosmic ray propagation, and provide some extra details to explain our method. The summary of our results is that the bulk of the parameter space of figure 4 (or equivalently figure 2) is allowed by current constraints. This is not a surprise: much of the parameter space consistent with the DM relic density corresponds to rather heavy m_χ at the several TeV, where current indirect searches do not yet constrain the thermal relic cross section. Indirect detection constraints do exclude, or make promising predictions for, the near-resonant SE regions seen in figure 4. If one accepts the assumption of a cusp DM density profile in the Milky Way Galactic Center, for example, then HESS gamma ray data already excludes much of the parameter region in the upper-left corner of the top panel of figure 4. Finally in 5.3 we end with a brief discussion of the constraints on dark matter self-interaction.

5.1 Antiprotons

The PAMELA satellite experiment reported a measurement of the high energy antiproton flux in interstellar space, extending up to $350\,\text{GeV}$ [30]. The PAMELA measurement is
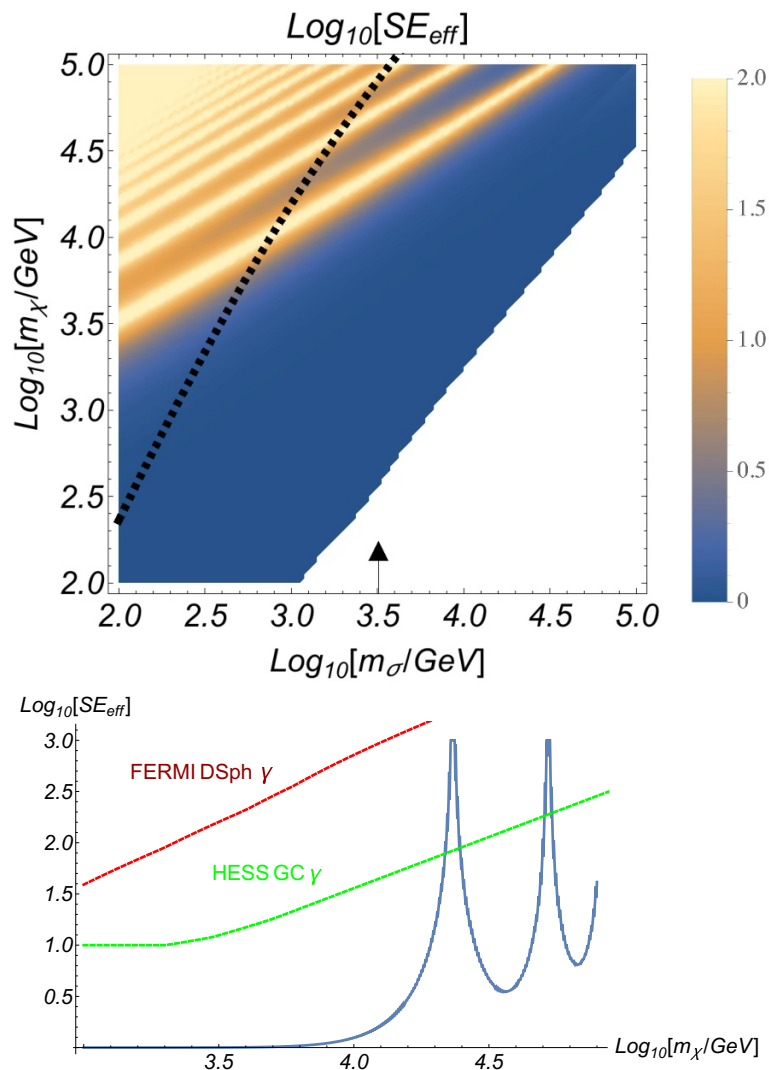
Figure 4. Top panel: Sommerfeld enhancement factor (SE) in the $\{m_\sigma, m_\chi\}$ plane. Above the dashed line $m_\sigma < f/10$, indicating fine-tuning. Bottom panel: SE vs. dark matter mass, fixing the dilaton mass to $m_\sigma = 3\,\mathrm{TeV}$ (marked on top panel with an arrow). The region above the red and green dashed lines is excluded by FERMI and HESS gamma ray observations (the latter depend strongly on assumptions regarding the DM distribution in the Galaxy; see section 5.2). The dark matter particles' relative velocity today is set to $v = 10^{-3}$.

consistent with model-independent calculations of the antiproton flux expected due to fragmentation of high energy primary cosmic ray nuclei on ambient interstellar gas in the Galaxy [31].

Following ref. [13], we derive a bound on the antiproton production in dark matter annihilation by imposing that the dark matter annihilation source of antiprotons in the local Galactic gas disc does not exceed the source due to the astrophysical production, in the energy range covered by the current measurements. The bound derived in this manner is independent of modeling assumptions regarding the propagation of charged cosmic rays
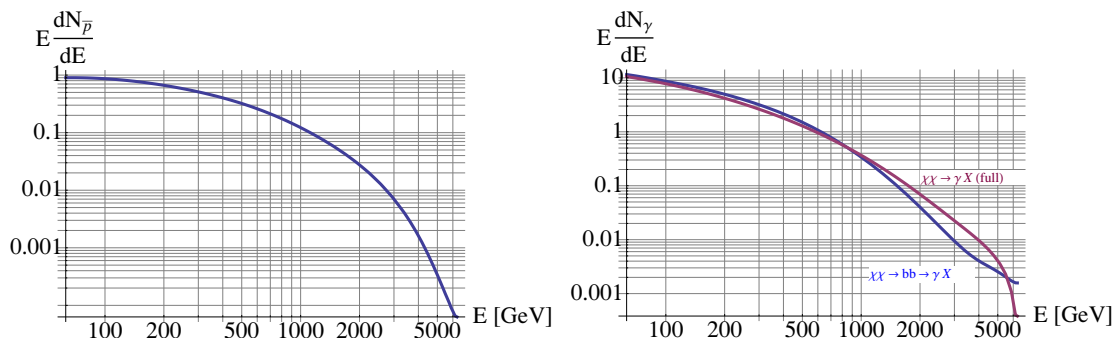
Figure 5. Left: differential $\bar{p}$ spectrum per DM annihilation, computed for $m_\chi = 6.3\,\text{TeV}$, $m_\sigma = 427\,\text{GeV}$, and $f = 6.2\,\text{TeV}$. Right: same for the gamma ray spectrum; the purple line shows the spectrum from the full annihilation process including all dominant partial channels ($\chi\chi \to WW, ZZ, tt, \sigma\sigma, \ldots$), while the blue line shows the spectrum due to $\chi\chi \to bb$ alone.

in the Galaxy. The bound is conservative because it does not include the possible additional contribution of DM annihilation in the cosmic ray halo that may extend well above and below the gas disc.

The injection rate density of antiprotons due to DM annihilation is given by

$$Q_{\bar{p},DM}(E) = \frac{1}{2} n_\chi^2 \langle \sigma v \rangle \frac{dN_{\bar{p}}}{dE} \approx 5 \times 10^{-36} \text{cm}^{-3}\text{s}^{-1}\text{GeV}^{-1} \times$$
$$\left(\frac{\rho_\chi}{0.4\,\text{GeVcm}^{-3}}\right)^2 \left(\frac{\langle \sigma v \rangle}{3 \times 10^{-26}\,\text{cm}^3\text{s}^{-1}}\right) \left(\frac{m_\chi}{1\,\text{TeV}}\right)^{-3} \left(m_\chi \frac{dN_{\bar{p}}}{dE}\right). \quad (5.2)$$

Here, $\rho_\chi = m_\chi n_\chi \approx 0.4\,\text{GeV}\,\text{cm}^{-3}$ is the DM mass density in the local halo and $\frac{dN_{\bar{p}}}{dE}$ is the differential antiproton spectrum per annihilation event. To compute $\frac{dN_{\bar{p}}}{dE}$ we use the code provided in ref. [32], that directly produces the differential $\bar{p}$ spectrum for the channels $\chi\chi \to WW, ZZ, hh, t\bar{t}$ accounting for the decay and hadronization of the intermediate unstable states. To include the contribution of $\chi\chi \to \sigma\sigma$ we proceed in two steps. First we use ref. [32] to calculate the $\bar{p}$ spectrum arising in the dilaton rest frame due to dilaton decay; define this spectrum by $\left[\frac{dN_{\bar{p}}}{dE}(E)\right]_{\sigma \to \bar{p}X}$. We then convolve the dilaton decay $\bar{p}$ spectrum with the isotropic boost factor of the σ in the DM annihilation center of mass frame, obtaining

$$\left[\frac{dN_{\bar{p}}}{dE}(E)\right]_{\chi\chi \to \sigma\sigma} = \frac{1}{\gamma_\sigma \beta_\sigma} \int_{\beta_\sigma^{-1}-1}^{\beta_\sigma^{-1}+1} \frac{dx}{x} \left[\frac{dN_{\bar{p}}}{dE}\left(\frac{E}{x\gamma_\sigma\beta_\sigma}\right)\right]_{\sigma \to \bar{p}X} \quad (5.3)$$

where $\gamma_\sigma = m_\chi/m_\sigma$ and $\beta_\sigma = \sqrt{1 - \gamma_\sigma^{-2}}$. We neglect DM annihilation into gluons, since the branching fraction of annihilation to this state is small compared to that of annihilation to quarks and massive gauge bosons. In the left panel of figure 5 we plot the differential flux of $\bar{p}$ from DM annihilation with $m_\chi = 6.3\,\text{TeV}$, $m_\sigma = 427\,\text{GeV}$, and $f = 6.2\,\text{TeV}$ reproducing the observed DM relic abundance.

The injection rate density due to primary cosmic rays colliding with interstellar gas in the disc is [31]

$$Q_{\bar{p},CR}(E) \approx 8.4 \times 10^{-33} \text{cm}^{-3} \text{s}^{-1} \text{GeV}^{-1} \times$$
$$\left(\frac{E}{100 \text{ GeV}}\right)^{-2.8} \left[1 - 0.22 \log_{10}^2 \left(\frac{E}{500 \text{ GeV}}\right)\right] \frac{J_p(1 \text{ TeV})}{J_{p,0}(1 \text{ TeV})}, \quad (5.4)$$

where $J_p(1 \text{ TeV})$ is the local proton flux sampled at $E = 1$ TeV and scaled to the measured value $J_{p,0}(1 \text{ TeV}) \approx 8 \times 10^{-9}$ GeV^{-1}cm^{-2}s^{-1}sr^{-1}. The uncertainties in the derivation of eq. (5.4) are at the $\sim$50% level. Our conservative bound on the DM annihilation rate amounts to imposing that the ratio $Q_{\bar{p},CR}(E)/Q_{\bar{p},DM}(E)$ is larger than unity for E in the range 10-300 GeV.

The basic result we find is that the model survives our antiproton constraint by a large margin, unless it lives right on top of an SE resonance. If the model is near an SE resonance, then a detectable rise in the antiproton flux at high energy is predicted. For DM mass below about ~ 10 TeV, the rise would be in tension with currently available $\bar{p}$ data and the model is observationally disfavored (again, only the region near an SE resonance, as seen in figure 4). For $m_\chi \gtrsim 10$ TeV, though, the rise in the $\bar{p}$ flux sets in at high energy with only a moderate effect in the energy range where current data exists. In this case, improved high energy cosmic ray measurements expected in the near future [33] may detect the model in the $\bar{p}$ flux.

We illustrate these findings in figure 6 where we plot the expected antiproton flux in our model near an SE resonance for two chosen points. The data points (last one being an upper bound) and the green curve denote the PAMELA data and the secondary astrophysics prediction, respectively. The red and magenta curves give an estimate of the antiproton flux that would occur for the parameter points $\{m_\chi = 6.3 \text{ TeV}, m_\sigma = 300 \text{ GeV}\}$ and $\{m_\chi = 31 \text{ TeV}, m_\sigma = 4.7 \text{ TeV}\}$, respectively, where the effective SE factor is $SE_{\text{eff}} \approx 10^3$ (fixing f to obtain the observed DM relic abundance).

Above we chose tuned points with large SE_{eff} to illustrate the possible $\bar{p}$ signal; as mentioned earlier, this large SE near the resonance peak can be damped somewhat by a more careful treatment of the relic abundance. However, we stress that the DM-induced signal depends on unknown cosmic ray propagation features. The red and magenta curves in figure 6 should be considered as a robust *lower bound* on the DM-induced flux. Considering disc+halo diffusion models [34], for example, the actual flux could be as high as a factor of ~ 100 above the result we show here.[6] A future detection of the model through cosmic ray $\bar{p}$ is therefore conceivable also away from SE resonance peaks.

5.2 Gamma rays

The FERMI gamma ray telescope reported limits on DM annihilation based on a stacking analysis of dwarf spheroidal galaxies [35]. The analysis is relatively insensitive to the assumed DM mass distribution in the target galaxies. Ref. [35] reports limits directly on the annihilation cross section for the specific channel $\chi\chi \to b\bar{b}$ as a function of the

---

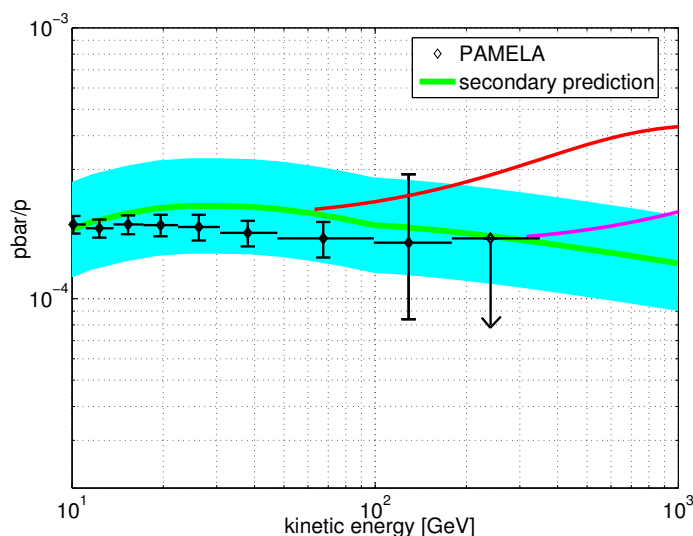[6]See appendix B of ref. [13] for a detailed discussion.

Figure 6. Antiproton flux with DM annihilation at a Sommerfeld factor resonance. Data points and green curve denote PAMELA data and secondary astrophysics prediction, respectively. Red and magenta curves give a lower estimate of the $\bar{p}$ flux with DM annihilation for the model parameter point with $\{m_\chi = 6.3 \text{ TeV}, m_\sigma = 300 \text{ GeV}\}$ and $\{m_\chi = 31 \text{ TeV}, m_\sigma = 4.7 \text{ TeV}\}$, respectively, where the SE factor is $SE_{\text{eff}} \approx 10^3$.

DM mass. Using the code of ref. [32] and following a similar method as that described above for the $\bar{p}$ spectrum calculation, we verified that the spectrum of continuum gamma rays obtained in our model agrees to within a factor of 2-3 with the gamma ray spectrum resulting from a pure $\chi\chi \to b\bar{b}$ channel. In what follows we therefore assume that the constraints quoted in [35] apply to our model directly. In the right panel of figure 5 we plot the differential gamma ray flux from DM annihilation with $m_\chi = 6.3 \text{ TeV}$, $m_\sigma = 427 \text{ GeV}$, and $f = 6.2 \text{ TeV}$ reproducing the observed DM relic abundance. The purple line shows the spectrum from the full annihilation process including all dominant partial channels $(\chi\chi \to WW, ZZ, tt, \sigma\sigma, \ldots)$, while the blue line shows the spectrum due to $\chi\chi \to bb$ alone.

We extrapolate the bound to $m_\chi = 100 \text{ TeV}$, using the scaling $m_\chi^{-2} \frac{dN_\gamma}{dE} \sim m_\chi^{-1}$ that applies for photon energies in the FERMI range, $E \lesssim 500 \text{ GeV} \ll m_\chi$. The resulting bound is illustrated by the red dashed line in the bottom panel of figure 4, focusing on a slice in the parameter space with $m_\sigma = 3 \text{ TeV}$.

Stronger, but more model-dependent limits are obtained from ground-based air-Cherenkov telescopes. The HESS gamma ray observatory reported limits on DM annihilation based on Galactic Center observations [36]. Due to the background subtraction method of the experiment, the analysis is not sensitive to shallow DM density profiles, and so the results are only applicable under the assumption of a cusp profile such as the Navaro-Frenk-White [37] distribution. Assuming a cusp distribution, neglecting the $\mathcal{O}(1)$ spectral difference between the $\chi\chi \to q\bar{q}$-induced gamma ray spectrum assumed in [36] and the actual spectrum in our model, and extrapolating their limits from $m_\chi = 10 \text{ TeV}$ up to $m_\chi = 100 \text{ TeV}$, we obtain the bound depicted by the green dashed line in the bottom panel of figure 4.

Finally, both FERMI [38] and HESS [39] reported limits on DM annihilation to a gamma ray line. We calculate the branching fraction $\langle\sigma v\rangle(\chi\chi \to \gamma\gamma)/\langle\sigma v\rangle(\text{total})$ using eq. (B.3). This branching fraction is very small in our model, reminiscent of the result for a heavy Higgs. Consequently the gamma ray line constraint is sub-dominant compared to the continuum emission bounds. We comment that the HESS limit [39] have recently been used to put significant pressure on supersymmetric Wino dark matter [40, 41]. This situation is not reproduced here; for the Wino example, the strong exclusion is primarily due to the presence of an electromagnetically charged state that is mass-degenerate with the neutral DM particle, amplifying the di-photon annihilation diagram. Without a special construction of this kind, our dilaton-mediated DM scenario passes the line searches unscathed.

5.3 Self-interaction and dipoles

Self-interaction of dark matter could occur in our model via two mechanisms. First, dilaton exchange leads to self-interaction cross sections per unit mass that scale roughly as $\sigma/m_\chi \sim m_\chi/f^4$ (assuming $m_\sigma \lesssim m_\chi$; otherwise there is an additional suppression by $(m_\chi/m_\sigma)^4$). Imposing the unitarity constraint as implemented in eq. (3.10), $m_\chi \lesssim 5f$, we have $\sigma/m_\chi < 600/m_\chi^3 \sim 10^{-10}\,(\text{TeV}/m_\chi)^3\,\text{cm}^2/\text{g}$. Throughout our relevant parameter space, this is many orders of magnitude below the observational constraints on the self interaction of dark matter, of order $\sim 1\,\text{cm}^2/\text{g}$ [42]. A second potential source of dark matter self-interaction could arise from the CFT side. Given the weakness of the astrophysical constraints, some amount of self-interaction is not excluded. However, without accounting for the details of the assumed (broken) CFT in which χ is embedded, we cannot address this issue quantitatively.

Similarly, limits from electric or magnetic moments are not constraining this model. Indeed, by assumption, our dark matter is only connected to the SM fields via dilaton exchange. Thus any magnetic or electric dipole moment must be induced through dilaton exchange (the latter necessitating, in addition, CP violation), with the exchanged particle being at the TeV scale, leading to induced couplings that are much too small to affect cosmological or astrophysical observations. For instance, considering the magnetic dipole moment (MDM) limit reported in [43], an MDM of $\mathcal{M} \sim 1/\text{GeV}$ is still easily consistent with cosmological data.

6 Conclusions

In this paper we explored the possibility that the dilaton could mediate dark matter annihilation. Such models have the appeal that the couplings are largely determined by scale invariance. The breaking scale of scale invariance f is fixed by requiring that the relic abundance matches the observed value, leaving the dark matter and dilaton masses as the main free parameters. We mapped the relevant $\{f, m_\chi, m_\sigma\}$ parameter space taking the various dark matter annihilation modes into account and imposing unitarity bounds. We showed that large regions of parameter space, with f, m_χ, m_σ all in the $\sim 1 - 10\,\text{TeV}$

range, can correctly reproduce the observed relic abundance. We find an upper bound $f \lesssim 30 - 100 \, \text{TeV}$, implying a similar bound on $m_{\sigma,\chi}$.

Collider searches for Higgs-like particles, including LHC, Tevatron and LEP analyses, put model dependent lower bounds on f for dilaton masses up to $\sim 1 \, \text{TeV}$. The collider bounds exclude dilaton-mediated dark matter for $m_\chi \lesssim 200 \, \text{GeV}$. Current direct detection experiments yield similar model dependent exclusions for the lower end of the mass spectrum, requiring $m_\chi \gtrsim 300 \, \text{GeV}$ for $m_\sigma \lesssim 300 \, \text{GeV}$. The predicted dark matter-nucleon elastic scattering cross section becomes independent of the dark matter mass for heavy dark matter.

Our analysis of indirect detection included antiproton and gamma ray data and shows that the bulk of the parameter space is consistent with the current constraints. A possible signal in high energy cosmic ray antiprotons could appear for favorable cosmic ray propagation scenario for models with parameters close to a Sommerfeld enhancement resonance. A promising avenue for probing the model all the way to very high DM mass is in high energy ground-based gamma ray measurements, see e.g. [44, 45] for recent reviews. For scalar or vector DM, future gamma ray experiments should detect or exclude the entire parameter space of the model.

Acknowledgments

Note added. While completing this project we became aware of [46] which investigates similar issues.

A   Collider bounds

As mentioned in the main text, in addition to the direct detection bounds there are also collider bounds from the LHC and earlier experiments. The dilaton (roughly) mimics a Higgs boson, with couplings to massive SM fields suppressed by the factor v/f compared to that of the Higgs and couplings to massless gauge bosons that involve contributions from the matter content of the conformal sector. Collider bounds on the dilaton can thus be obtained by recasting the results of direct production limits from Higgs boson searches. We use the HiggsBound [47–49] code version 4.1.2, that incorporates all the currently available experimental analyses from LEP, the Tevatron, and the LHC [47–49].

The resulting collider bounds on the conformal symmetry breaking scale f as a function of the dilaton mass is presented in figure 7 for the two benchmark models A and B defined in
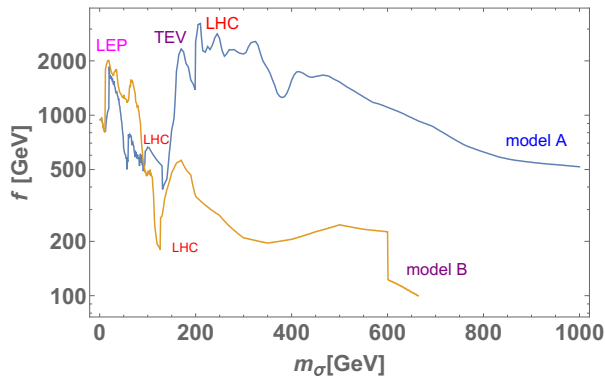
Figure 7. 95% C.L. collider exclusion limit on the scale of conformal symmetry breaking, f, with respect to m_σ for our benchmark models A and B.

section 2. In obtaining these bounds we assumed, for simplicity, no invisible decay channels for the dilaton. We can see that the collider bounds are strongly model dependent: model A has a large coupling to gluons, and thus is very strongly constrained throughout the parameter space relevant for LHC kinematics. Model B has small couplings to gluons and photons, and is only weakly constrained for dilaton masses above $200\,\mathrm{GeV}$.

The resulting bound on f can be turned into a bound on m_χ using figure 2. For example the $f \gtrsim 2\,\mathrm{TeV}$ bound for $m_\sigma \lesssim 400\,\mathrm{GeV}$ in model A implies $m_\chi \gtrsim 300\,\mathrm{GeV}$, with the exception for a narrow resonance region.

B Additional annihilation channels

B.1 Scalar dark matter

Annihilation to fermions of mass m_ψ:

$$\sigma v(\chi\chi \to \bar{\psi}\psi) \simeq \frac{m_\psi^2 m_\chi \left(m_\chi^2 - m_\psi^2\right)^{3/2}}{\pi f^4 |4m_\chi^2 - m_\sigma^2 - i\mathrm{Im}\left(\Pi(4m_\chi^2)\right)|^2} \tag{B.1}$$

Annihilation to a real scalar of mass m_h:

$$\sigma v(\chi\chi \to hh) \simeq \frac{m_\chi m_h^4 \sqrt{m_\chi^2 - m_h^2}}{4\pi f^4 |4m_\chi^2 - m_\sigma^2 - i\mathrm{Im}\left(\Pi(4m_\chi^2)\right)|^2} \tag{B.2}$$

While annihilation to photons is negligible for the relic abundance calculation, it is important for indirect detection. We get

$$\sigma v(\chi\chi \to \gamma\gamma) \simeq \frac{3m_\chi^6 \alpha_{\mathrm{EM}}^2 c_{\mathrm{EM}}^2}{16\pi^3 f^4 |4m_\chi^2 - m_\sigma^2 - i\mathrm{Im}\left(\Pi(4m_\chi^2)\right)|^2} \tag{B.3}$$

where $c_{\rm EM}$ encodes the coupling of photons to dilaton:

$$c_{\rm EM} = \left(F_W(x_W) - \sum_f N_c Q_f^2 F_f(x_f) + b_{\rm IR}^{\rm (EM)} - b_{\rm UV}^{\rm (EM)} \right) \tag{B.4}$$

$$x_i = \frac{m_i^2}{m_\chi^2} \tag{B.5}$$

$$F_W(x) = 2 + 3x + 3x(2-x)f(x) \tag{B.6}$$

$$F_f(x) = 2x[1 + (1-x)f(x)] \tag{B.7}$$

$$f(x) = \begin{cases} \arcsin(1/\sqrt{x})^2 & : x \geq 1 \\ -\frac{1}{4}\left[\log\left(\frac{1+\sqrt{x-1}}{1-\sqrt{x-1}}\right) - i\pi\right]^2 & : x < 1 \end{cases} \tag{B.8}$$

B.2 Fermion dark matter

Annihilation to fermions of mass m_ψ:

$$\sigma v(\bar{\chi}\chi \to \bar{\psi}\psi) \simeq v^2 \frac{m_\psi^2 m_\chi \left(m_\chi^2 - m_\psi^2\right)^{3/2}}{8\pi f^4 |4m_\chi^2 - m_\sigma^2 - i{\rm Im}\left(\Pi(4m_\chi^2)\right)|^2} \tag{B.9}$$

Annihilation to a real scalar of mass m_h:

$$\sigma v(\bar{\chi}\chi \to hh) \simeq v^2 \frac{m_\chi m_h^4 \sqrt{m_\chi^2 - m_h^2}}{32\pi f^4 |4m_\chi^2 - m_\sigma^2 - i{\rm Im}\left(\Pi(4m_\chi^2)\right)|^2} \tag{B.10}$$

B.3 Vector dark matter

Annihilation to fermions of mass m_ψ:

$$\sigma v(\chi\chi \to \bar{\psi}\psi) \simeq \frac{m_\psi^2 m_\chi \left(m_\chi^2 - m_\psi^2\right)^{3/2}}{3\pi f^4 |4m_\chi^2 - m_\sigma^2 - i{\rm Im}\left(\Pi(4m_\chi^2)\right)|^2} \tag{B.11}$$

Annihilation to a real scalar of mass m_h:

$$\sigma v(\chi\chi \to hh) \simeq \frac{m_\chi m_h^4 \sqrt{m_\chi^2 - m_h^2}}{12\pi f^4 |4m_\chi^2 - m_\sigma^2 - i{\rm Im}\left(\Pi(4m_\chi^2)\right)|^2} \tag{B.12}$$

C Dilaton decay channels

For decay to a real scalar of mass m_h we get

$$\Gamma_\sigma(\sigma \to hh) = \frac{m_h^4}{8\pi m_\sigma f^2}\sqrt{1 - \frac{4m_h^2}{m_\sigma^2}} \tag{C.1}$$

For decay to fermions we get

$$\Gamma_\sigma(\sigma \to \bar{\psi}\psi) = \frac{m_\sigma m_\psi^2}{8\pi f^2}\left(1 - \frac{4m_\psi^2}{m_\sigma^2}\right)^{3/2} \tag{C.2}$$

References

[1] C.G. Callan Jr., S.R. Coleman and R. Jackiw, *A New improved energy - momentum tensor*, [*Annals Phys.* **59** (1970) 42](#) [INSPIRE].

[2] C. Csáki, M. Graesser, L. Randall and J. Terning, *Cosmology of brane models with radion stabilization*, [*Phys. Rev.* **D 62** (2000) 045015](#) [hep-ph/9911406] [INSPIRE].

[3] G.F. Giudice, R. Rattazzi and J.D. Wells, *Graviscalars from higher dimensional metrics and curvature Higgs mixing*, [*Nucl. Phys.* **B 595** (2001) 250](#) [hep-ph/0002178] [INSPIRE].

[4] C. Csáki, M.L. Graesser and G.D. Kribs, *Radion dynamics and electroweak physics*, [*Phys. Rev.* **D 63** (2001) 065002](#) [hep-th/0008151] [INSPIRE].

[5] C. Csáki, J. Hubisz and S.J. Lee, *Radion phenomenology in realistic warped space models*, [*Phys. Rev.* **D 76** (2007) 125015](#) [arXiv:0705.3844] [INSPIRE].

[6] W.D. Goldberger, B. Grinstein and W. Skiba, *Distinguishing the Higgs boson from the dilaton at the Large Hadron Collider*, [*Phys. Rev. Lett.* **100** (2008) 111802](#) [arXiv:0708.1463] [INSPIRE].

[7] Y. Eshel, S.J. Lee, G. Perez and Y. Soreq, *Shining Flavor and Radion Phenomenology in Warped Extra Dimension*, [*JHEP* **10** (2011) 015](#) [arXiv:1106.6218] [INSPIRE].

[8] B. Bellazzini, C. Csáki, J. Hubisz, J. Serra and J. Terning, *A Higgslike Dilaton*, [*Eur. Phys. J.* **C 73** (2013) 2333](#) [arXiv:1209.3299] [INSPIRE].

[9] LUX collaboration, D.S. Akerib et al., *First results from the LUX dark matter experiment at the Sanford Underground Research Facility*, [*Phys. Rev. Lett.* **112** (2014) 091303](#) [arXiv:1310.8214] [INSPIRE].

[10] XENON100 collaboration, E. Aprile et al., *Dark Matter Results from 225 Live Days of XENON100 Data*, [*Phys. Rev. Lett.* **109** (2012) 181301](#) [arXiv:1207.5988] [INSPIRE].

[11] CDMS collaboration, R. Agnese et al., *Silicon Detector Dark Matter Results from the Final Exposure of CDMS II*, [*Phys. Rev. Lett.* **111** (2013) 251301](#) [arXiv:1304.4279] [INSPIRE].

[12] Y. Bai, M. Carena and J. Lykken, *Dilaton-assisted Dark Matter*, [*Phys. Rev. Lett.* **103** (2009) 261803](#) [arXiv:0909.1319] [INSPIRE].

[13] K. Agashe, K. Blum, S.J. Lee and G. Perez, *Astrophysical Implications of a Visible Dark Matter Sector from a Custodially Warped-GUT*, [*Phys. Rev.* **D 81** (2010) 075012](#) [arXiv:0912.3070] [INSPIRE].

[14] Z. Chacko and R.K. Mishra, *Effective Theory of a Light Dilaton*, [*Phys. Rev.* **D 87** (2013) 115006](#) [arXiv:1209.3022] [INSPIRE].

[15] Z. Chacko, R.K. Mishra and D. Stolarski, *Dynamics of a Stabilized Radion and Duality*, [*JHEP* **09** (2013) 121](#) [arXiv:1304.1795] [INSPIRE].

[16] B. Bellazzini, C. Csáki, J. Hubisz, J. Serra and J. Terning, *A Naturally Light Dilaton and a Small Cosmological Constant*, [*Eur. Phys. J.* **C 74** (2014) 2790](#) [arXiv:1305.3919] [INSPIRE].

[17] F. Coradeschi, P. Lodone, D. Pappadopulo, R. Rattazzi and L. Vitale, *A naturally light dilaton*, *JHEP* **11** (2013) 057 [arXiv:1306.4601] [INSPIRE].

[18] PLANCK collaboration, P.A.R. Ade et al., *Planck 2013 results. XVI. Cosmological parameters*, *Astron. Astrophys.* **571** (2014) A16 [arXiv:1303.5076] [INSPIRE].

[19] K. Griest and M. Kamionkowski, *Unitarity Limits on the Mass and Radius of Dark Matter Particles*, *Phys. Rev. Lett.* **64** (1990) 615 [INSPIRE].

[20] J.L. Feng, M. Kaplinghat and H.-B. Yu, *Sommerfeld Enhancements for Thermal Relic Dark Matter*, *Phys. Rev.* **D 82** (2010) 083525 [arXiv:1005.4678] [INSPIRE].

[21] P.J. Fox, R. Harnik, J. Kopp and Y. Tsai, *Missing Energy Signatures of Dark Matter at the LHC*, *Phys. Rev.* **D 85** (2012) 056011 [arXiv:1109.4398] [INSPIRE].

[22] P. Junnarkar and A. Walker-Loud, *Scalar strange content of the nucleon from lattice QCD*, *Phys. Rev.* **D 87** (2013) 114510 [arXiv:1301.1114] [INSPIRE].

[23] Y. Bai, P.J. Fox and R. Harnik, *The Tevatron at the Frontier of Dark Matter Direct Detection*, *JHEP* **12** (2010) 048 [arXiv:1005.3797] [INSPIRE].

[24] J.R. Ellis, K.A. Olive and C. Savage, *Hadronic Uncertainties in the Elastic Scattering of Supersymmetric Dark Matter*, *Phys. Rev.* **D 77** (2008) 065026 [arXiv:0801.3656] [INSPIRE].

[25] K. Blum, *Cosmic ray propagation time scales: lessons from radioactive nuclei and positron data*, *JCAP* **11** (2011) 037 [arXiv:1010.2836] [INSPIRE].

[26] J. Hisano, S. Matsumoto and M.M. Nojiri, *Explosive dark matter annihilation*, *Phys. Rev. Lett.* **92** (2004) 031303 [hep-ph/0307216] [INSPIRE].

[27] J. Hisano, S. Matsumoto, M.M. Nojiri and O. Saito, *Non-perturbative effect on dark matter annihilation and gamma ray signature from galactic center*, *Phys. Rev.* **D 71** (2005) 063528 [hep-ph/0412403] [INSPIRE].

[28] S. Cassel, *Sommerfeld factor for arbitrary partial wave processes*, *J. Phys.* **G 37** (2010) 105009 [arXiv:0903.5307] [INSPIRE].

[29] T.R. Slatyer, *The Sommerfeld enhancement for dark matter with an excited state*, *JCAP* **02** (2010) 028 [arXiv:0910.5713] [INSPIRE].

[30] A.G. Mayorov, O. Adriani, G. Barbarino, G.A. Bazilevskaia, R. Belotti et al., *Antiprotons of galactic cosmic radiation in the PAMELA experiment*, *Bull. Russ. Acad. Sci. Phys.* **77** (2013) 602 [INSPIRE].

[31] B. Katz, K. Blum and E. Waxman, *What can we really learn from positron flux 'anomalies'?*, *Mon. Not. Roy. Astron. Soc.* **405** (2010) 1458 [arXiv:0907.1686] [INSPIRE].

[32] M. Cirelli, G. Corcella, A. Hektor, G. Hutsi, M. Kadastik et al., *PPPC 4 DM ID: A Poor Particle Physicist Cookbook for Dark Matter Indirect Detection*, *JCAP* **03** (2011) 051 [*Erratum ibid.* **1210** (2012) E01] [arXiv:1012.4515] [INSPIRE].

[33] A. Kounine, *The Alpha Magnetic Spectrometer on the International Space Station*, *Int. J. Mod. Phys.* **E 21** (2012) 1230005.

[34] V. Ginzburg, V. Dogiel, V. Berezinsky, S. Bulanov and V. Ptuskin, *Astrophysics of cosmic rays*, Amsterdam, Netherlands: North-Holland, 1990, pg. 534.

[35] FERMI-LAT collaboration, M. Ackermann et al., *Dark matter constraints from observations of 25 Milky Way satellite galaxies with the Fermi Large Area Telescope*, *Phys. Rev.* **D 89** (2014) 042001 [arXiv:1310.0828] [INSPIRE].

[36] HESS collaboration, A. Abramowski et al., *Search for a Dark Matter annihilation signal from the Galactic Center halo with H.E.S.S*, *Phys. Rev. Lett.* **106** (2011) 161301 [arXiv:1103.3266] [INSPIRE].

[37] J.F. Navarro, C.S. Frenk and S.D.M. White, *The Structure of cold dark matter halos*, *Astrophys. J.* **462** (1996) 563 [astro-ph/9508025] [INSPIRE].

[38] LAT collaboration, M. Ackermann et al., *Fermi LAT Search for Dark Matter in Gamma-ray Lines and the Inclusive Photon Spectrum*, *Phys. Rev.* **D 86** (2012) 022002 [arXiv:1205.2739] [INSPIRE].

[39] HESS collaboration, A. Abramowski et al., *Search for Photon-Linelike Signatures from Dark Matter Annihilations with H.E.S.S.*, *Phys. Rev. Lett.* **110** (2013) 041301 [arXiv:1301.1173] [INSPIRE].

[40] T. Cohen, M. Lisanti, A. Pierce and T.R. Slatyer, *Wino Dark Matter Under Siege*, *JCAP* **10** (2013) 061 [arXiv:1307.4082] [INSPIRE].

[41] J. Fan and M. Reece, *In Wino Veritas? Indirect Searches Shed Light on Neutralino Dark Matter*, *JHEP* **10** (2013) 124 [arXiv:1307.4400] [INSPIRE].

[42] S. Tulin, H.-B. Yu and K.M. Zurek, *Beyond Collisionless Dark Matter: Particle Physics Dynamics for Dark Matter Halo Structure*, *Phys. Rev.* **D 87** (2013) 115007 [arXiv:1302.3898] [INSPIRE].

[43] C. Dvorkin, K. Blum and M. Kamionkowski, *Constraining Dark Matter-Baryon Scattering with Linear Cosmology*, *Phys. Rev.* **D 89** (2014) 023519 [arXiv:1311.2937] [INSPIRE].

[44] S. Funk, *Indirect Detection of Dark Matter with gamma rays*, arXiv:1310.2695 [INSPIRE].

[45] M. Doro, *A decade of dark matter searches with ground-based Cherenkov telescopes*, *Nucl. Instrum. Meth.* **A 742** (2014) 99 [arXiv:1404.5017] [INSPIRE].

[46] A. Efrati, E. Kuflik, S. Nussinov, Y. Soreq and T. Volansky, *Constraining the Higgs-Dilaton with LHC and Dark Matter Searches*, arXiv:1410.2225 [INSPIRE].

[47] P. Bechtle, O. Brein, S. Heinemeyer, G. Weiglein and K.E. Williams, *HiggsBounds: Confronting Arbitrary Higgs Sectors with Exclusion Bounds from LEP and the Tevatron*, *Comput. Phys. Commun.* **181** (2010) 138 [arXiv:0811.4169] [INSPIRE].

[48] P. Bechtle, O. Brein, S. Heinemeyer, G. Weiglein and K.E. Williams, *HiggsBounds 2.0.0: Confronting Neutral and Charged Higgs Sector Predictions with Exclusion Bounds from LEP and the Tevatron*, *Comput. Phys. Commun.* **182** (2011) 2605 [arXiv:1102.1898] [INSPIRE].

[49] P. Bechtle, O. Brein, S. Heinemeyer, O. Stal, T. Stefaniak et al., *Recent Developments in HiggsBounds and a Preview of HiggsSignals*, PoS(CHARGED 2012)024 [arXiv:1301.2345] [INSPIRE].